

## Discrete molecular dynamics simulations of peptide aggregation

S. Peng,<sup>1</sup> F. Ding,<sup>1</sup> B. Urbanc,<sup>1</sup> S. V. Buldyrev,<sup>1</sup> L. Cruz,<sup>1</sup> H. E. Stanley,<sup>1</sup> and N. V. Dokholyan<sup>2</sup>

<sup>1</sup>Center for Polymer Studies and Department of Physics, Boston University, Boston, Massachusetts 02215, USA

<sup>2</sup>Department of Biochemistry and Biophysics, University of North Carolina at Chapel Hill, Chapel Hill, North Carolina 27599, USA

(Received 6 November 2003; published 29 April 2004)

We study the aggregation of peptides using the discrete molecular dynamics simulations. Specifically, at temperatures above the  $\alpha$ -helix melting temperature of a single peptide, the model peptides aggregate into a multilayer parallel  $\beta$ -sheet structure. This structure has an interstrand distance of 4.8 Å and an intersheet distance of 10 Å, which agree with experimental observations. Our model explains these results as follows: hydrogen-bond interactions give rise to the interstrand spacing in  $\beta$  sheets, while  $G\bar{o}$  interactions between side chains make  $\beta$  strands parallel to each other and allow  $\beta$  sheets to pack into layers. An important feature of our results is that the aggregates contain free edges, which may allow for further aggregation of model peptides to form elongated fibrils.

DOI: 10.1103/PhysRevE.69.041908

PACS number(s): 87.14.Ee, 87.15.By, 87.15.He, 87.15.Kg

### I. INTRODUCTION

Protein misfolding and polypeptide aggregation are a focus of interdisciplinary statistical physics because of their relevance to amyloid diseases such as Alzheimer's disease, Parkinson's disease, and Huntington's disease. Even though polypeptides related to these diseases share no sequence or secondary structure similarity, they can aggregate into insoluble fibrils which share some structural features. These fibrils are typically 100 Å in diameter, and several thousand angstroms in length [1]. X-ray diffraction studies [2,3] reveal the common structural features for these amyloid fibrils: the presence of a 4.7–4.8 Å interstrand spacing along the fibril axis and a 9–10 Å intersheet spacing perpendicular to the fibril axis [4,5]. Although advances have been made toward understanding the structural characteristics of the fibrils and the mechanism of fibril formation, our knowledge of the detailed fibrillar structure and mechanisms of amyloid assembly is limited.

Computer simulation studies with coarse-grained peptide models have been helpful to reveal the general principles of folding and aggregation. Recently, lattice Monte Carlo simulations show that an increased proportion of  $\beta$  sheets in the individual peptides promotes the formation of misfolded aggregates in multipolypeptide systems [6]. However, lattice models may not be reliable due to the drastic reduction of the conformational space when entropies or local geometries play crucial roles in cases involving transition of secondary structures, such as the aggregation phenomena. Therefore, off-lattice molecular dynamics provides a more realistic way to study the aggregation mechanism at the atomic level. Since the continuous all-atom molecular dynamics simulations with realistic force fields in a physiological solution are not fast enough to monitor a complete aggregation process from monomers to fully formed fibrils, a discrete molecular dynamics (DMD) algorithm [7,8] has been implemented to study protein folding thermodynamics and protein folding kinetics [9]. This computationally fast and dynamically realistic simulation technique has also been applied to study the aggregation of a small number of Src SH3 domain proteins [10] and the competition of refolding and aggregation of

four-helix bundles [11]. Recently developed off-lattice Monte Carlo simulations [12] may also serve as an alternative methodology to lattice Monte Carlo simulations.

Here we study the aggregation of a large number of peptides. We choose 40 amino acid amyloid  $\beta$  peptide [ $A\beta_{1-40}$  [13], protein data bank (PDB) [14] access code 1BA4] which is associated with Alzheimer's disease, to construct model peptides. Our results show that model peptides can aggregate into multilayer  $\beta$ -sheet structures with free edges [15] which may enable further fibrillar elongation. The computed diffraction pattern of our simulated multilayer  $\beta$  sheet is consistent with experimental observations [16,17].

### II. METHODS

#### A. Two-bead model

##### 1. Geometry of model peptide: beads and permanent bonds

We model each amino acid in the  $A\beta_{1-40}$  peptide by two beads— $C_\alpha$  bead representing backbone atoms and  $C_\beta$  bead representing side chain atoms (for glycine,  $C_\beta$  is absent). Each bead has an index  $i$  indicating the position of amino acid in the sequence starting from the  $N$  terminus. The geometry of the peptide is modeled by applying permanent bonds among these beads [18]. These bonds include covalent bonds between  $C_{\alpha i}$  and  $C_{\beta i}$ , peptide bonds between  $C_{\alpha i}$  and  $C_{\alpha(i\pm 1)}$ , additional constraints between  $C_{\beta i}$  and  $C_{\alpha(i\pm 1)}$ , and also between  $C_{\alpha i}$  and  $C_{\alpha(i\pm 2)}$  (Fig. 1). These additional constraints are introduced to model angular restrictions between side chains and the backbone.

All permanent bonds are realized by infinitely high potential well interactions between the related beads [8],

$$V_{ij}^{bond} = \begin{cases} 0, & D_{ij}(1 - \sigma_{ij}) < |r_i - r_j| < D_{ij}(1 + \sigma_{ij}) \\ +\infty & \text{otherwise.} \end{cases} \quad (1)$$

Here  $D_{ij}$  is the bond length between beads  $i$  and  $j$ , and  $\sigma_{ij}$  is the relative deviation of this bond length. The average lengths for these bonds can be obtained from statistical analysis of distances within the  $A\beta_{1-40}$  NMR structures

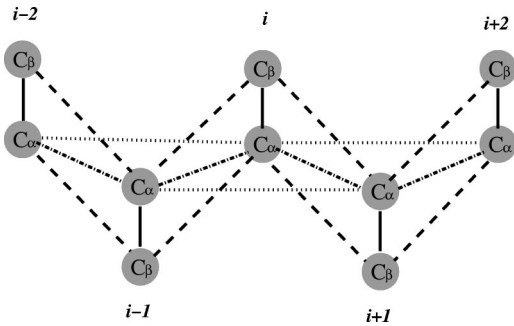


FIG. 1. Schematic diagram of two-bead model. Each amino acid in the  $A\beta_{1-40}$  peptide is represented by two beads:  $C_\alpha$  bead represents backbone atoms and  $C_\beta$  bead represents side chain atoms ( $C_\beta$  is absent for glycine). The geometry of the peptide is modeled by applying permanent bonds among these beads: covalent bonds (bold lines), peptide bonds (dash-dotted lines), and additional constraints (dashed and dotted lines). Interactions between side chains are modeled by  $G\bar{o}$  potentials between  $C_\beta$  beads, and interactions between backbone atoms are modeled by hydrogen-bond interactions between  $C_\alpha$  beads.

[13]. Table I presents the average lengths and their relative deviations [19] used in our model.

### 2. Interactions between $C_\beta$ beads: $G\bar{o}$ model

Typically the  $G\bar{o}$  potentials [7,20] are used to model proteins with well-defined globular native states. Side chains which form contacts in the native state (native contacts) experience attractive  $G\bar{o}$  potential. However,  $A\beta_{1-40}$  peptide is “natively unfolded.” NMR studies suggest that in hydrophobic environments the  $A\beta_{1-40}$  peptide assumes mostly  $\alpha$ -helical conformation [13]. Figure 2 (a) shows one of these NMR structures. Therefore, we apply  $G\bar{o}$  potentials to preserve this well-defined, mostly  $\alpha$ -helical structure of the  $A\beta_{1-40}$  peptide. In our two-bead model a native contact is defined when two  $C_\beta$  beads are closer than  $D^{G\bar{o}} = 7.5 \text{ \AA}$  within the NMR structure of the  $A\beta_{1-40}$  peptide. All the  $C_\beta$  beads cannot be closer than the hard-core distance  $D_{HC}^{G\bar{o}} = 4.5 \text{ \AA}$ . In particular, the structure-specific  $G\bar{o}$  potentials make the side chains indexed by  $i$  within the  $\alpha$ -helix region of  $A\beta_{1-40}$  peptide attract side chains  $i \pm 2, i \pm 3$ , and  $i \pm 4$ . Figure 2(b) shows the native contact map for the NMR structure of  $A\beta_{1-40}$  peptide shown in Fig. 2(a).

To study the aggregation we need to simulate also the interactions between different peptides. We apply  $G\bar{o}$  potentials for  $C_\beta$  beads in different peptides by an assumption that two amino acids which interact with each other in a single peptide will interact in the same way in different peptides.

TABLE I. Permanent bonds in the two-bead model.

Bond	Bond length ( $\text{\AA}$ )	Deviation (%)
$C_{\alpha i} - C_{\beta i}$	1.55	2.4
$C_{\alpha i} - C_{\alpha(i \pm 1)}$	3.82	3.1
$C_{\beta i} - C_{\alpha(i \pm 1)}$	4.66	6.5
$C_{\alpha i} - C_{\alpha(i \pm 2)}$	5.65	14.8

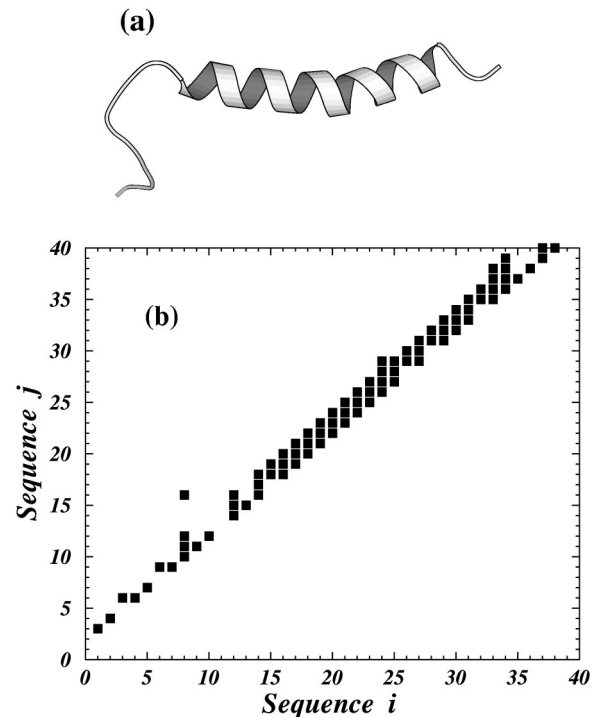


FIG. 2. (a) The NMR structure of  $A\beta_{1-40}$  peptide [13] used to construct the two-bead model peptide with  $G\bar{o}$  potentials and hydrogen-bond interactions. The picture is created with the program Molscrip [31]. (b) The contact map for structure (a). Note that the  $\alpha$ -helical region is formed by amino acids 15–36 (Q15-V36).

For example, amino acids 16 and 19 form a native contact in the NMR structure. Thus, amino acids at 16 and 19 of peptide 1 will experience attractive  $G\bar{o}$ -type interaction with amino acids 19 and 16 of the peptide 2, respectively. The strength of  $G\bar{o}$  interactions is set to unity,  $\epsilon^{G\bar{o}} = 1$ .

### 3. Interactions between $C_\alpha$ beads: hydrogen bond

For many globular proteins it has been observed that the number of backbone hydrogen bonds for each amino acid does not exceed two [21]. Also, whenever two hydrogen bonds are formed in a particular peptide block they are approximately parallel to each other. In order to incorporate these two facts in our model we introduce two criteria for hydrogen-bond formation: (i) that each  $C_\alpha$  bead can form up to two effective hydrogen bonds, and (ii) that the two hydrogen bonds formed by the same  $C_\alpha$  bead must be approximately parallel.

We set the hydrogen-bond interaction range between two  $C_\alpha$  beads to  $D^{HB} = 5.0 \text{ \AA}$ , and their hard-core distance to  $D_{HC}^{HB} = 4.0 \text{ \AA}$ . We use the following procedure in order to satisfy the criteria for the hydrogen-bond formation: when two  $C_\alpha$  beads,  $A$  and  $B$ , come to a distance  $D^{HB}$ , we check for any existing hydrogen-bond partners of  $A$  and  $B$ . If both beads  $A$  and  $B$  have no existing hydrogen partners they can form a hydrogen bond automatically. If one of the beads, for example  $A$ , already has one partner,  $A_1$ , and the distance between the bead  $A_1$  and the bead  $B$  is within the range of  $8.7\text{--}10 \text{ \AA}$  (i.e., the angle between vectors  $\vec{AA}_1$  and  $\vec{AB}$  is

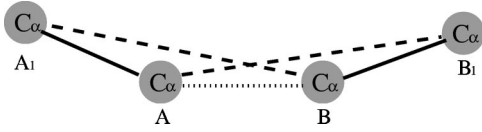


FIG. 3. Model of a hydrogen bond. Existing hydrogen bonds  $AA_1$  and  $BB_1$  are shown in bold lines. When the beads  $A$  and  $B$  come to a distance  $5 \text{ \AA}$ , a new hydrogen bond (dotted line) may form if the distances  $A_1B$  and  $B_1A$  satisfy inequalities  $8.7 \text{ \AA} \leq A_1B \leq 10.0 \text{ \AA}$  and  $8.7 \text{ \AA} \leq B_1A \leq 10.0 \text{ \AA}$ . If the bond  $AB$  is formed, the auxiliary bonds  $A_1B$  and  $B_1A$  (dashed lines) are formed simultaneously. These bonds can fluctuate within the interval  $8.7\text{--}10 \text{ \AA}$  and cannot be broken unless beads  $A$  and  $B$  move away from each other to a distance  $5 \text{ \AA}$ . If the beads  $A$  and  $B$  have enough kinetic energy to leave the hydrogen-bond attraction well, their velocities are changed in order to conserve energy and momentum, and the hydrogen bond  $AB$  is destroyed simultaneously with the auxiliary bonds  $A_1B$  and  $B_1A$ . The velocities of  $A_1$  and  $B_1$  do not change at the moment of forming or destroying of hydrogen bond  $AB$ . Analogously, if one of the hydrogen bonds,  $A_1A$  or  $B_1B$ , breaks before hydrogen bond  $AB$ , the corresponding auxiliary bond  $A_1B$  or  $B_1A$  also breaks.

within the range  $120^\circ\text{--}180^\circ$ ), the bead  $A$  can form another hydrogen bond with bead  $B$  provided that either the bead  $B$  has no existing hydrogen bonds or its single hydrogen-bond partner,  $B_1$ , has a distance with bead  $A$  in the range  $8.7\text{--}10 \text{ \AA}$  (see Fig. 3). If one of beads  $A$  and  $B$  or both already have two hydrogen-bond partners, the pair will proceed with a hard-core collision without forming a new hydrogen bond. When a new hydrogen bond is formed between beads  $A$  and  $B$ , new hydrogen-bond partners are recorded for these two beads, and whenever a bead gets two hydrogen-bond partners an auxiliary bond is formed between these two partners. Every auxiliary bond can fluctuate within the range  $8.7\text{--}10 \text{ \AA}$  to keep two hydrogen bonds within the angle  $120^\circ\text{--}180^\circ$  and it cannot be broken unless one of the two hydrogen bonds is broken. A hydrogen bond between beads  $A$  and  $B$  can be broken when these two beads move away from each other to a distance of  $D^{HB}$  and their kinetic energies are higher than  $\epsilon^{HB}$ . When a hydrogen bond is formed or broken, the velocities of the beads  $A$  and  $B$  change in order to conserve energy and momentum, such that their kinetic energy increases or decreases by the value  $\epsilon^{HB}$ . We set  $\epsilon^{HB} = 3$  as it was chosen in Ref. [10] for Src SH3 domain.

### B. Computed diffraction

For the typical conformation of  $A_{B_{1-40}}$  peptide aggregation structure, we calculate the intensity of diffraction pattern using the elastic diffraction formula [10] in order to compare with experimental results [16,17].

$$I(\vec{k}_f) = \left| \sum_j \exp[i(\vec{k}_f - \vec{k}_i) \cdot \vec{r}_j] \right|^2, \quad (2)$$

where  $\vec{k}_i$  is the wave vector of the incident x ray,  $\vec{k}_f$  is the wave vector of the outgoing x ray,  $\vec{r}_j$  is the position vector of  $j$ th bead, and the summation is taken over all the  $C_\alpha$  and  $C_\beta$  beads in the structure.

We chose  $x$  axis perpendicular to the  $\beta$  sheets, and  $y$  axis along the fibrillar axis which is perpendicular to the  $\beta$  strands in the  $\beta$  sheets [Fig. 7(a)]. The incoming x ray with  $1 \text{ \AA}$  wavelength goes along  $z$  axis and the diffraction pattern is collected on a  $x$ - $y$  plane behind the aggregate sample. The deflecting angle,  $\theta = \cos^{-1}(\vec{k}_f \cdot \vec{k}_i / k^2)$ , ranges from 0.05 to 0.25 in radians in order to detect the periodicity of  $4\text{--}20 \text{ \AA}$  in the aggregate structure. Since amyloid fibrils consist of bundles of  $\beta$ -sheet chains which are twisted along the  $y$  axis, there is no preferred orientation in the  $x$ - $z$  plane in the x-ray diffraction experiments. We rotate the structure candidate around the  $y$  (fibrillar) axis  $n$  times by angle  $2\pi/n$  and add all the diffraction intensities to obtain a final pattern. We take  $n = 20$  in the present study.

### III. RESULTS FOR A SINGLE PEPTIDE

As an initial test of our model peptide, we perform DMD simulations of a single peptide to test whether a peptide with random coil conformation recovers the observed NMR structure. The model peptide is slowly cooled from  $T_i = 1.00$  (temperature is measured in units of  $\epsilon^{G\sigma}/k_B$ ), which is high enough to render the peptide as a random coil, to different target temperatures  $T_t = 0.60, 0.55, \dots, 0.25$ . For each target temperature we make ten trials starting with different initial conformations. When  $T_t \leq 0.40$ , the segment Q15-V36 adopts an  $\alpha$  helix or two pieces of left-handed and right-handed  $\alpha$  helices. This artifact is observed because our simplified two-bead model does not distinguish between different handedness. At  $T_t = 0.40$ , the  $N$  terminus adopts mostly a random coil conformation. As  $T_t < 0.35$ , the model peptide starts to approach its ground state which is an  $\alpha$  helix with a single handedness along the entire peptide chain. Therefore, as expected within a certain temperature range around  $T = 0.40$  during the cooling process the model peptide adopts partial  $\alpha$ -helical conformation similar to the observed one in NMR experiments.

We also study the equilibrium behavior of a single model peptide at different temperatures by measuring the heat capacity as a function of temperature. At each sampled temperature we start with a ground-state conformation and perform DMD for  $10^6$  simulation time units to equilibrate the system, followed by additional  $10^7$  time units for the calculations. The time unit is  $l_0 \sqrt{m_c / \epsilon^{G\sigma}}$ , where  $l_0 \equiv 1 \text{ \AA}$  is the unit of length and the mass of a carbon atom  $m_c$  is the unit of mass in the DMD simulations. Figures 4(a) and 4(b) show the potential energy and heat capacity as a function of temperature for a single model peptide, respectively. The melting of  $\alpha$  helix is noncooperative which can be concluded from the broad peak between  $T_N \approx 0.35$  and  $T_m \approx 0.55$  in the heat capacity curve [Fig. 4(b)].  $T_N$  corresponds to the structural transition from an  $\alpha$  helix to a random coil for the first 14 amino acids starting from the  $N$  terminus, while  $T_m$  corresponds to the melting of the  $\alpha$  helix in the segment Q15-V36.  $T_m$  is higher than  $T_N$  because there are more attractions among the side chains in the segment Q15-V36.

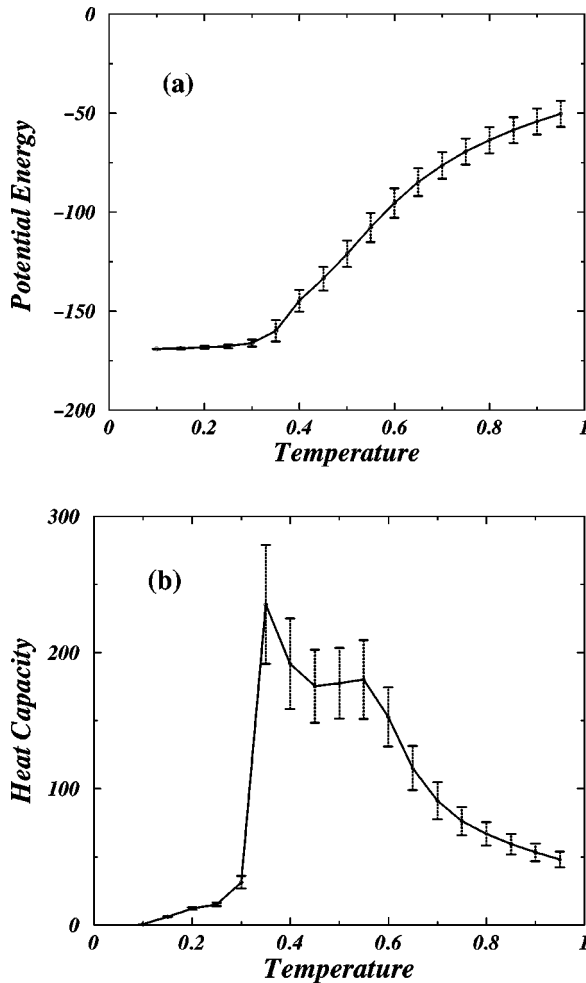


FIG. 4. Temperature dependence of (a) potential energy and (b) heat capacity for a single two-bead  $A\beta_{1-40}$  model peptide with  $G\bar{o}$  potentials and hydrogen-bond interactions. The calculations are based on the DMD simulations of  $10^7$  time units for each sampled temperature. The units for temperature, potential energy, and heat capacity are  $\epsilon^{G\bar{o}}/k_B$ ,  $\epsilon^{G\bar{o}}$ , and  $k_B$ , respectively.

#### IV. RESULTS FOR MULTIPLE PEPTIDES

In the study of aggregation of many identical peptides, we perform simulations of 28 peptides in a cubic box with the edge of 200 Å and periodic boundary conditions. Initially, all the peptides are placed on a grid and randomly oriented [see Fig. 5(a)]. Then we equilibrate the system at various temperatures:  $T_f=0.4, 0.5, \dots, 1.20$ .

At temperatures lower than the melting temperature  $T_m$  of a single peptide, peptides in our model aggregate into amorphous structures where individual peptides preserve part of their  $\alpha$ -helical segments as in Fig. 5(b). When the temperature is higher than  $T_m$ , peptides start to aggregate into more ordered structures. When the temperature is higher than 1.10, there is no stable aggregate (this threshold temperature depends on the peptide concentration). At a temperature range between 0.55 and 1.10, the model peptides can aggregate into multilayer  $\beta$ -sheet structures. Figures 6(a) and 6(b) show the time evolution of the conformation obtained from DMD simulation at temperature 0.90. In Fig. 7(a) we illus-

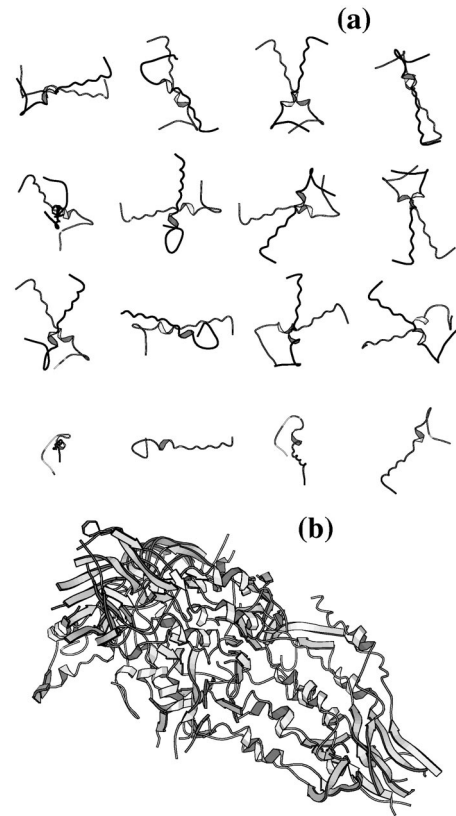


FIG. 5. DMD simulation of 28 peptides at temperature 0.5: (a) initially, all peptides in an original randomly oriented NMR conformation are placed on a grid. (b) An amorphous aggregate obtained by DMD simulation at this temperature of 0.5. The numbers of  $\alpha$ -helical and  $\beta$ -sheet hydrogen bonds are 166 and 240, respectively. The simulation shows that part of the  $\alpha$ -helical segments are preserved during the aggregation at this temperature.

trate the setup of diffraction computation and in Fig. 7(b) we present the calculated diffraction pattern. The relative sharp and intense 4.8 Å meridional reflection corresponds to the periodic packing of  $\beta$  strands along the fibril axis, and the

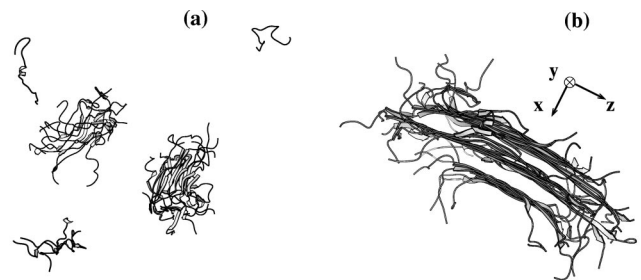


FIG. 6. DMD simulation of 28 peptides at temperature 0.90. Initial conformation is the same as Fig. 5(a). After 500 time units all peptides acquire random coil conformation characteristics for  $T=0.90$  (data not shown). (a) Intermediate conformation at temperature 0.90 after  $10^4$  DMD simulation time units. (b) Three-layer parallel  $\beta$ -sheet structure formed after  $2.5 \times 10^5$  DMD simulation time units. This  $\beta$ -sheet structure contains free edges which may allow for further aggregation of model peptides along the y axis, which is perpendicular to the plane of the figure.

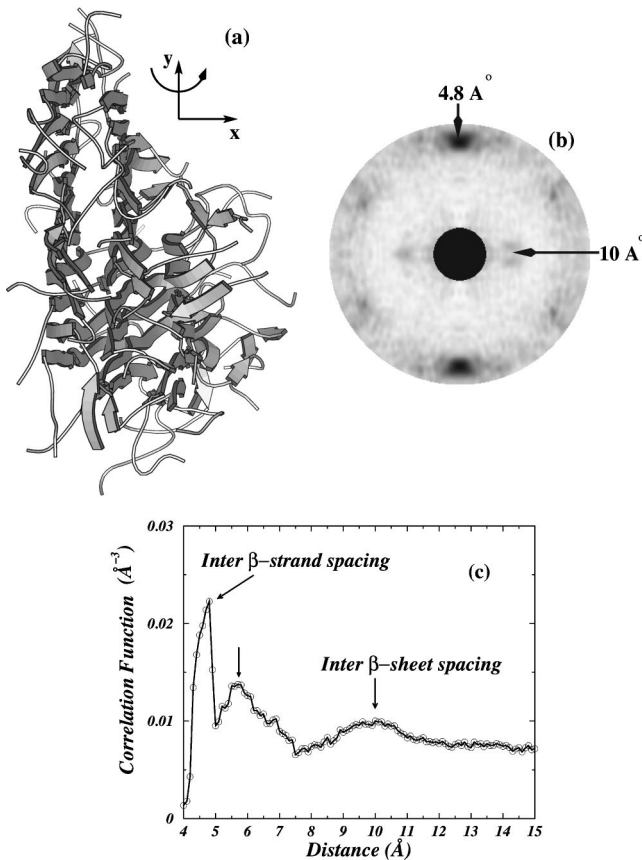


FIG. 7. (a) The setup of diffraction pattern computation for the three-layer  $\beta$ -sheet aggregate formed by 28 peptides shown in Fig. 6(b) at a different perspective. The scattering occurs along  $z$  axis which is perpendicular to the plane of the figure. (b) Computed diffraction pattern collected on a  $x$ - $y$  plane behind the aggregate. The pattern is averaged over 20 patterns obtained by successive rotation of the aggregate around  $y$  axis by  $18^\circ$ . (c) Pair correlation function for the same aggregate, where peaks around  $4.8 \text{ \AA}$  and  $10 \text{ \AA}$  correspond to interstrand spacing and intersheet spacing, respectively. And the peak around  $5.7 \text{ \AA}$  is mainly from the correlation between neighboring  $C_\beta$  beads.

weaker  $10 \text{ \AA}$  equatorial reflection corresponds to the distance between  $\beta$  sheets. In Fig. 7(c) we show the calculated pair correlation function for the same  $\beta$ -sheet structure. The peaks around  $4.8 \text{ \AA}$  and  $10 \text{ \AA}$  correspond to the average interstrand and intersheet spacings, respectively.

In order to study the thermostability of this three-layer  $\beta$ -sheet structure, we slowly increase the temperature to  $T = 2.0$  which is high enough to melt the aggregate. Figures 8(a) and 8(b) show the time evolution of temperature and the temperature dependence of potential energy of the system during melting and dissociation of the  $\beta$ -sheet structure, respectively. As temperature increases from  $0.90$ , the aggregate becomes less stable. At temperature around  $T = 1.15 \pm 0.05$ , aggregate starts to dissociate. At temperatures higher than  $T_d = 1.20 \pm 0.05$  the dissociation completes.

We can assume that the temperature  $0.9$  at which the aggregation of  $\beta$  sheet is observed corresponds to physiological temperature  $310 \text{ K}$ . At this temperature our single model peptide exists in a random coil conformation, which corre-

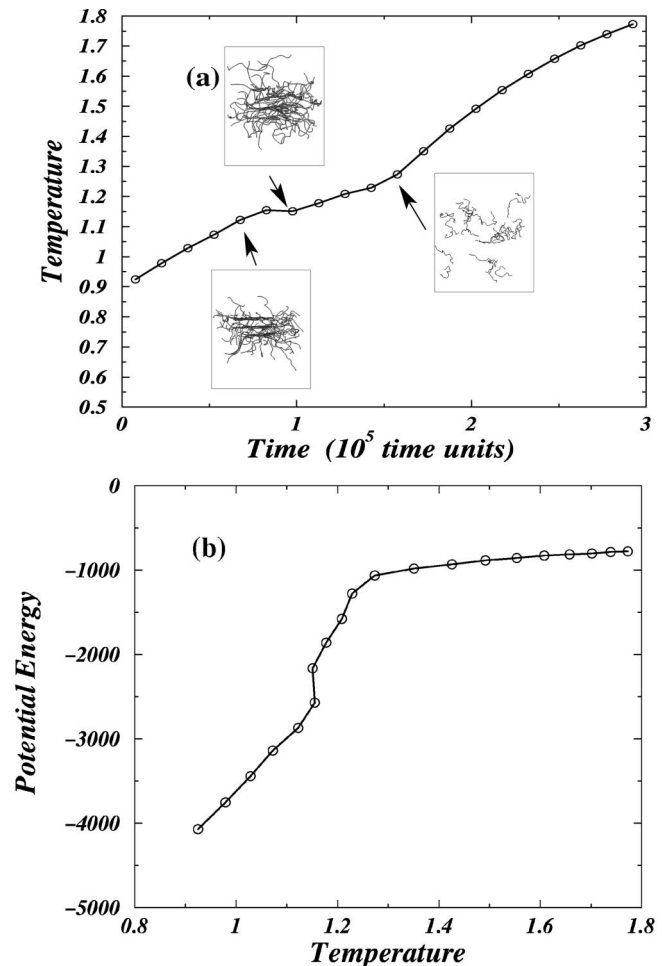


FIG. 8. The melting of the three-layer  $\beta$ -sheet structure of 28  $A\beta$  peptides [Fig. 6(c)]. (a) Time evolution of the temperature when the three-layer  $\beta$  sheet is warmed up slowly from temperature  $0.90$ – $2.00$ . The dissociation temperature is  $T_d = 1.20 \pm 0.05$ . The insets are the conformations at different times/temperatures. Note that the third one shows a completely dissociated conformation in three dimensions. (b) The temperature dependence of potential energy. The units for time, temperature, and potential energy are  $l_0 \sqrt{m_c} / \epsilon^{G\bar{\sigma}}$ ,  $\epsilon^{G\bar{\sigma}} / k_B$ , and  $\epsilon^{G\bar{\sigma}}$ , respectively.

sponds to experimental observations [22,23] that in aqueous solution at physiological temperatures  $A\beta_{1-40}$  peptides adopt mostly  $\beta$ -sheet and coil conformations. The temperature of the  $\beta$ -sheet dissociation  $1.2$  corresponds to  $413 \text{ K}$ . Temperature  $T = 0.40$  at which our model peptide acquires  $\alpha$ -helical conformation corresponds to very low physical temperatures which cannot be observed experimentally.

## V. DISCUSSION AND CONCLUSION

In the test of our coarse-grained model of  $A\beta_{1-40}$  peptide, we find that the model peptide most resembles the NMR structure of  $A\beta_{1-40}$  peptide around  $T = 0.40$ . The existence of an optimal temperature range for protein refolding is also observed in experiments [24] and other coarse-grained models [25]. Below  $T = 0.40$  the  $N$ -terminal region of our model peptide mostly adopts an  $\alpha$ -helical conformation. However,

in the present study of aggregation we are focused on temperatures above 0.40 as the peptides are generally partially or completely unfolded to initiate the aggregation process [26].

In studies of multiple peptides, we demonstrate that peptides aggregate into amorphous structures [Fig. 5(b)] around  $T=0.50$  or multiple-layer  $\beta$ -sheet structures [Fig. 6(b)] around  $T=0.90$ . In the amorphous structures, individual peptides tend to preserve part of the  $\alpha$ -helical structure, while in the  $\beta$ -sheet structures the  $\beta$  strands tend to be parallel. Since the  $G\bar{o}$  interaction for an  $\alpha$  helix favors the formation of contacts between amino acids  $i$  and  $i\pm 3$ , the aggregates with a parallel alignment have lower potential energies.

There are caveats due to the simplicity of the two-bead model used in our study. Each amino acid is represented by only two beads, which do not allow for an accurate description of the backbone. The backbone in this model is too flexible, which introduces some artifacts into conformations of aggregates composed of small number of peptides at low temperatures, such as dimers, trimers, and tetramers.

An additional problem is that the chiral symmetry of each amino acid is not considered in this model. As a result, we observe two  $\alpha$  helices with opposite handedness. As the  $A\beta_{1-40}$  NMR structure consists of two  $\alpha$  helices and a hinge in between, there are four low-energy states with combinations of different handedness within the region of  $\alpha$  helices at  $T=0.40$ . The conformations with mixed handedness appear with lower probabilities since they have higher potential

energies due to the loss of native contacts and hydrogen bonds in between the two  $\alpha$  helices of different handedness.

Also, due to the simplicity of the two-bead model, we do not account for specific structural features of  $A\beta_{1-40}$  peptides, such as the salt bridge between D23 and K28 [27]. For the same reason, we cannot expect to explain the differences in aggregation pathways between  $A\beta_{1-40}$  and  $A\beta_{1-42}$  alloforms [28], nor study subtle aggregation differences due to amino acid substitutions [29]. We show that the DMD algorithm using a simplified peptide model can reproduce the formation of  $\beta$ -sheet structures of 28 peptides with free edges for further fibrillization. Our study shows that it is possible to investigate in detail the aggregation of several dozens of peptides using DMD simulations and the coarse-grained model for peptide structure. Both the number of peptides and the complexity of the model [30] can be significantly increased within realistic computational constraints. Thus, we regard this study as a first step toward developing a realistic model of  $A\beta$  peptide aggregation.

#### ACKNOWLEDGMENTS

We thank J.M. Borreguero, C.K. Hall, A. Lam, and S. Yun for discussions, and the Memory Ride Foundation for support. We would like to specially thank E.I. Shakhnovich for his advice and discussions. N.V.D. acknowledges the support of the UNC-CH Research Council Grant.

- 
- [1] J.D. Sipe and A.S. Cohen, *J. Struct. Biol.* **130**, 88 (2000).  
 [2] E.D. Eanes and G.G. Glenner, *J. Histochem. Cytochem.* **16**, 673 (1968).  
 [3] M. Sunde, L.C. Serpell, M. Bartlam, P.E. Fraser, M.B. Pepys, and C.C. Blake, *J. Mol. Biol.* **273**, 729 (1997).  
 [4] L. Bonar, A.S. Cohen, and M.M. Skinner, *Proc. Soc. Exp. Biol. Med.* **131**, 1373 (1969).  
 [5] D.A. Kirschner, C. Abraham, and D.J. Selkoe, *Proc. Natl. Acad. Sci. U.S.A.* **83**, 503 (1986).  
 [6] D. Bratko and H.W. Blanch, *J. Chem. Phys.* **118**, 5185 (2003).  
 [7] Y. Zhou and M. Karplus, *Proc. Natl. Acad. Sci. U.S.A.* **94**, 14429 (1997).  
 [8] N.V. Dokholyan, S.V. Buldyrev, H.E. Stanley, and E.I. Shakhnovich, *Folding Des.* **3**, 577 (1998).  
 [9] J.M. Borreguero, N.V. Dokholyan, S.V. Buldyrev, E.I. Shakhnovich, and H.E. Stanley, *J. Mol. Biol.* **318**, 863 (2002).  
 [10] F. Ding, N.V. Dokholyan, S.V. Buldyrev, H.E. Stanley, and E.I. Shakhnovich, *J. Mol. Biol.* **324**, 851 (2002).  
 [11] A.V. Smith and C.K. Hall, *J. Mol. Biol.* **312**, 187 (2001).  
 [12] J. Shimada, E.L. Kussell, and E.I. Shakhnovich, *J. Mol. Biol.* **308**, 79 (2001).  
 [13] M. Coles, W. Bicknell, A.A. Watson, D.P. Fairlie, and D.J. Craik, *Biochemistry* **37**, 11064 (1998).  
 [14] H.M. Berman, J. Westbrook, Z. Feng, G. Gilliland, T.N. Bhat, H. Weissig, I.N. Shindyalov, and P.E. Bourne, *Nucleic Acids Res.* **28**, 235 (2000).  
 [15] J.S. Richardson and D.C. Richardson, *Proc. Natl. Acad. Sci. U.S.A.* **99**, 2754 (2002).  
 [16] S.B. Malinchik, H. Inouye, K.E. Szumowski, and D.A. Kirschner, *Biophys. J.* **74**, 537 (1998).  
 [17] L.C. Serpell, *Biochim. Biophys. Acta* **1502**, 16 (2000).  
 [18] F. Ding, N.V. Dokholyan, S.V. Buldyrev, H.E. Stanley, and E.I. Shakhnovich, *Biophys. J.* **83**, 3525 (2002).  
 [19] In a DMD simulation, the speed of the simulation depends on the number of collisions. If a bond width is too small, most of the computing time will be wasted on the collisions due to small local vibrations of this bond. However, if the bond width too big, the model would not be realistic enough.  
 [20] H. Taketomi, Y. Ueda, and N.  $G\bar{o}$ , *Int. J. Pept. Protein Res.* **7**, 445 (1975).  
 [21] Bifurcated hydrogen bonding is very rare and is not considered here.  
 [22] O. Gursky and S. Aleshkov, *Biochim. Biophys. Acta* **1476**, 93 (2000).  
 [23] C. Soto, E.M. Castano, B. Frangione, and N.C. Inestrosa, *J. Biol. Chem.* **270**, 3063 (1995).  
 [24] R. Jaenicke and R. Seckler, *Adv. Protein Chem.* **50**, 1 (1997).  
 [25] A.V. Smith and C.K. Hall, *Proteins: Struct., Funct., Genet.* **44**, 376 (2001).  
 [26] F. Chiti, M. Stefani, N. Taddei, G. Ramponi, and C.M. Dobson, *Nature (London)* **424**, 805 (2003).

- [27] A.T. Petkova, Y. Ishii, J.J. Balbach, O.N. Antzutkin, R.D. Leapman, F. Delaglio, and R. Tycko, Proc. Natl. Acad. Sci. U.S.A. **99**, 16742 (2002).
- [28] G. Bitan, M.D. Kiritadze, A. Lomakin, S.S. Vollers, G.B. Benedek, and D.B. Teplow, Proc. Natl. Acad. Sci. U.S.A. **100**, 330 (2003).
- [29] G. Bitan, S.S. Vollers, and D.B. Teplow, J. Biol. Chem. **278**, 34882 (2003).
- [30] F. Ding, J.M. Borreguero, S.V. Buldyrev, H.E. Stanley, and N.V. Dokholyan, Proteins: Struct., Funct., Genet. **53**, 220 (2003).
- [31] P.J. Kraulis, J. Appl. Crystallogr. **24**, 946 (1991).